Available online at www.sciencedirect.com

jmr&t Journal of Materials Research and Technology

journal homepage: www.elsevier.com/locate/jmrt

Original Article

Investigation of exit-hole repairing on dissimilar aluminum-copper friction stir welded joints

Kush Mehta [a,b,*], *Antonello Astarita* [c], *Pierpaolo Carlone* [d], *Roberta Della Gatta* [c], *Hardik Vyas* [b], *Pedro Vilaça* [a], *Fausto Tucci* [d]

[a] *Department of Mechanical Engineering, School of Engineering, Aalto University, Espoo, Finland*
[b] *Department of Mechanical Engineering, School of Technology, Pandit Deendayal Energy University, Gandhinagar, India*
[c] *Department of Chemical, Materials and Production Engineering, University of Naples "Federico II", P.le Tecchio 80, 80125, Italy*
[d] *Department of Industrial Engineering, University of Salerno, Via Giovanni Paolo II 132, Fisciano, Italy*

ARTICLE INFO

Article history:
Received 11 February 2021
Accepted 6 June 2021
Available online 11 June 2021

Keywords:
Dissimilar joints
Exit-hole
Friction stir welding
Hardness
Microstructure
Refill
Repair
Strength

ABSTRACT

Exit-holes in friction stir welded dissimilar aluminum-copper (Al–Cu) joints are repaired by using probeless tools, forcing the surrounding material to fill the exit-hole cavity. The repair by refilling the same base materials is performed in two steps using probeless tools of different diameters. In this study, two different conditions are investigated, keeping the processing parameters constant and varying the tool shoulder diameters. Namely, the repair is performed using a two steps sequence of probeless tools with shoulder diameters of: (1) 12 and 19 mm, and (2) 12 and 27 mm. The refill action is achieved using only the base materials. A comprehensive experimental campaign, including tensile tests, microhardness measurements, scanning electron microscopy and energy dispersive x-ray spectroscopy investigations, have been conducted to evaluate the effectiveness of the repairing. The results showed that the usage of probeless tool is an effective strategy to repair the exit-hole of dissimilar Al–Cu friction stir welds, with exclusive contribution from the same Al and Cu base materials in the cavity of the exit-hole. The original FSW joint with exit-hole, with a diameter of about 8 mm, repaired by shoulder diameters of 12 and 19 mm exhibited ultimate tensile strength about 13% higher than the values provided by the samples taken in the steady-state region of the weld bead The maximum and minimum hardness of the repairing zone made with shoulder diameters of 12 and 19 mm are 240 and 80 HV0.1, respectively, which are within the range of the friction stir welded regions indicated in previous studies.

* Corresponding author.
E-mail addresses: kush.mehta@aalto.fi, kush_2312@yahoo.com (K. Mehta).
https://doi.org/10.1016/j.jmrt.2021.06.019

1. Introduction

Welding dissimilar materials is an interesting engineering solution that leads to number of advantages such as light-weight, cost savings, hybrid properties and structures, as well as increased performance and more [1–3]. Aluminum (Al) and copper (Cu) welding is one of these dissimilar combinations that is used for appealing applications in different industries, including e-mobility in automotive, aerospace components, electronic components, electric wires, electric bus bars and mechanical components [2,4–6]. The Al–Cu applications are still developing and coming up with new possibilities, such as multi-material Al–Cu structural components with novel channel on Al rib and simultaneously welded to Cu thin plate by hybrid channeling [7]. Besides, the welding of Al–Cu is challenging due to the different properties of these two materials. Friction stir welding (FSW), that is originally developed for joining difficult-to-melt structural alloys such as Al-alloys and Cu-alloys, among others [8–17], and related technological variants, have proved ability to provide effective joints between Al–Cu materials due to solid state nature [18–22]. In FSW-based processes, a non-consumable tool is applied to govern stirring-mixing mechanism for welding, wherein the material flow is influenced by the profile of tool's probe and the processing temperature of the workpiece materials [23,24]. However, at the end of the weld cycle and during retraction phase of the tool, a cavity is created in the adjoined material, whose shape corresponds to the tool probe's dynamic volume [18,25–28]. This open cavity is named exit-hole [29] and has a depth corresponding to the penetration of the processed zone, which in butt joint design typically corresponds to the thickness of the welded workpieces. This exit-hole is one of the three major issues, namely (i) back support, (ii) weld thinning and (iii) keyhole defect/exit-hole, that need to be addressed to broaden the scope of FSW in manufacturing field [30]. Therefore, it is considered as a disadvantage related to the FSW and its variants, as this exit-hole zone of the welds cannot be subjected to in-service component due to issues of stress and/or corrosion concentration. Therefore, different approaches are applied to deal with this exit-hole presence [30]. One frequent approach to overcome the influence of the exit-hole is the placement of additional run-off tabs that need to be removed after welding, wherein the exit-hole is formed on these tabs [31]. The material wastage is a concern in addition to the time needed for secondary cutting operation with this conventional approach of run-off tabs. Other approaches are developed, such as (i) filling of exit-hole by inserting an external bit/consumable plug of material inside the exit-hole, known as friction bit joining/friction plug welding [32–34], (ii) friction forming using die and subsequent forging from revert side [35–37], (iii) self-refilling by adjustable probe in friction stir welding set-up allows vertical material movement to fill the exit-hole from probe's vertical movement [38], and (iv) repairing of exit-hole by filling additional consumable material inside the exit-hole cavity by secondary processes using tungsten inert gas welding, or friction plug welding [32,33,39]. One of the easiest, cost effective and robust approaches to repair exit-hole is the use of probeless non consumable tools consisting of higher diameter of shoulder as compared to exit-hole diameter [40,41]. The material adjacent to exit-hole is plastically deformed and forged to fill the exit-hole using probeless non consumable tools with appropriate combination of rotating speed of tool and rate of plunging.

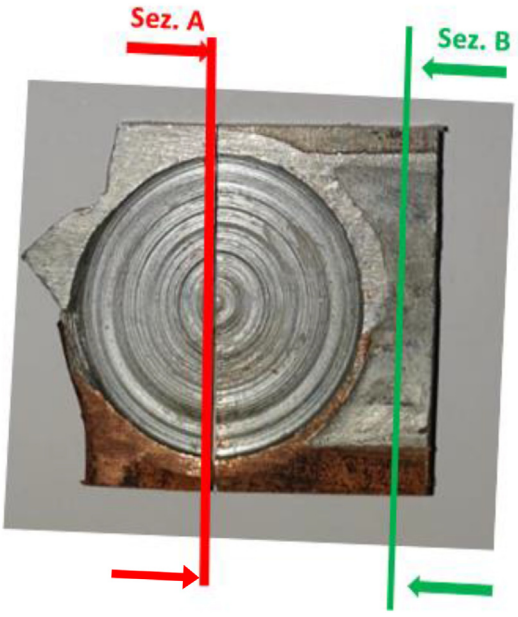

Fig. 1 – Samples extraction indication for cross sectional analysis of macrographs, microstructures, and hardness measurements.

Ji et al. [35] applied probeless tools to repair exit-hole of AZ31B FSW. They claimed more than 90% of matching tensile strength and elongation for repaired zone as compared to defect free welded zone. Ji et al. [36] also studied the same concept of exit-hole repairing using probeless tools on FSW of 7N01-T4, wherein they claimed more than 80% of tensile strength and 90% elongation for repaired zone as compared to FS welded zone. Wen et al. [37] repaired ZL210 aluminum alloy using probeless tools and obtained equivalent tensile strength as compared to FS welded joints. Mehta et al. [41] repaired exit-hole for dissimilar AA6061-AZ31B FSW using probeless tools and successfully repaired exit-hole with intrigued material mixing between AA6061 and AZ31B material, wherein tensile strength of repaired zone is 124% overmatching to the FS welded zone. The concept of probeless tools for repairing is extended as friction spot extrusion welding [42,43] and

Table 1 – Chemical composition of base materials (wt.%) [given by vendor and verified by elemental analysis].

Alloy	Al	Mg	Cu	Cr	Fe	Mn	Si	Zn	Ti	O	Impurities
AA6061-T6	Balance	1.03	0.17	0.11	0.30	0.12	0.56	0.08	0.03	–	0.04
ETP Cu	–	–	99.9	–	–	–	–	–	–	0.009	Balance

modified friction stir clinching [44,45], wherein protuberance leveling of surface is obtained eliminating exit-hole. The exit-hole repairing using probeless tools is limitedly investigated for dissimilar materials combination that may be due to metallurgical problems of material mixing challenges. To the best of authors' knowledge, the combination of Al–Cu materials welded by FSW have not being investigated so far for exit-hole repairing using probeless tools. Therefore, it is worthwhile to present a study on materials mixing and mechanical properties of exit-hole repaired zone in case of dissimilar Al–Cu FSW. In the present investigation, the exit-hole of dissimilar FSW of AA6061 to ETP Cu is repaired by probeless tools in two steps with two different conditions of tool's shoulder diameters. The materials mixing and mechanical properties of repaired zone and FS welded zone are studied in this investigation.

2. Materials and methods

Dissimilar materials of AA6061-T6 and electrolytic tough pitch copper (ETP Cu), with thickness of 6 mm, purchased from Bharat Aerospace Metals, are used as base materials in the present investigation. Table 1 presents chemical composition of the base materials. FSW process is performed on base materials in butt joint configuration with previously developed processing conditions, such as tool design with shoulder diameter of 27 mm and cylindrical M8 threaded probe profile, and process parameters of rotational speed 1500 rpm, travel speed 50 mm/min, tool probe offset 2 mm towards Al side, and 2° tilt angle. Good mechanical properties and stable FSW conditions are obtained from investigation in [18,19,21]. The exit-hole, of about 8 mm diameter, of FS welded samples is repaired by probeless tools in two different steps, wherein processing parameters such as rotational speed 1500 rpm, rate of plunge 3 mm/min and tool hold time 2 min are kept constant while varying shoulder diameters. In the repairing process, two different processing conditions are investigated by varying tool shoulder diameters, having flat shoulder surface's profile for all the repairing tools. In Condition 1, the first step of repairing is performed by probeless tool of 12 mm shoulder diameter and second step by probeless tool of 19 mm shoulder diameter. In Condition 2 the first step of repairing is performed by probeless tool of 12 mm shoulder diameter, and

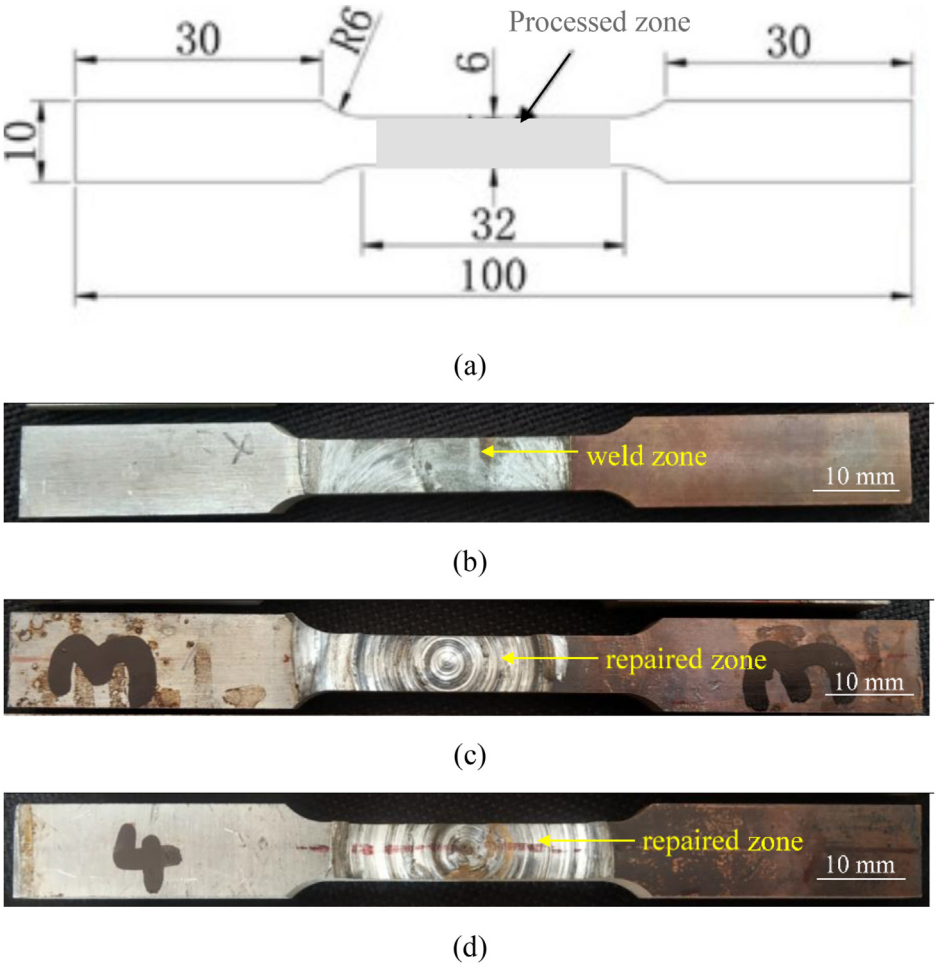

Fig. 2 – (a) Tensile testing specimens' dimensions as per ASTM E8 standards, extracted from (b) FS welded specimen, (c) repaired by shoulder diameters of 12 and 19 mm, and (d) repaired by shoulder diameters of 12 and 27 mm.

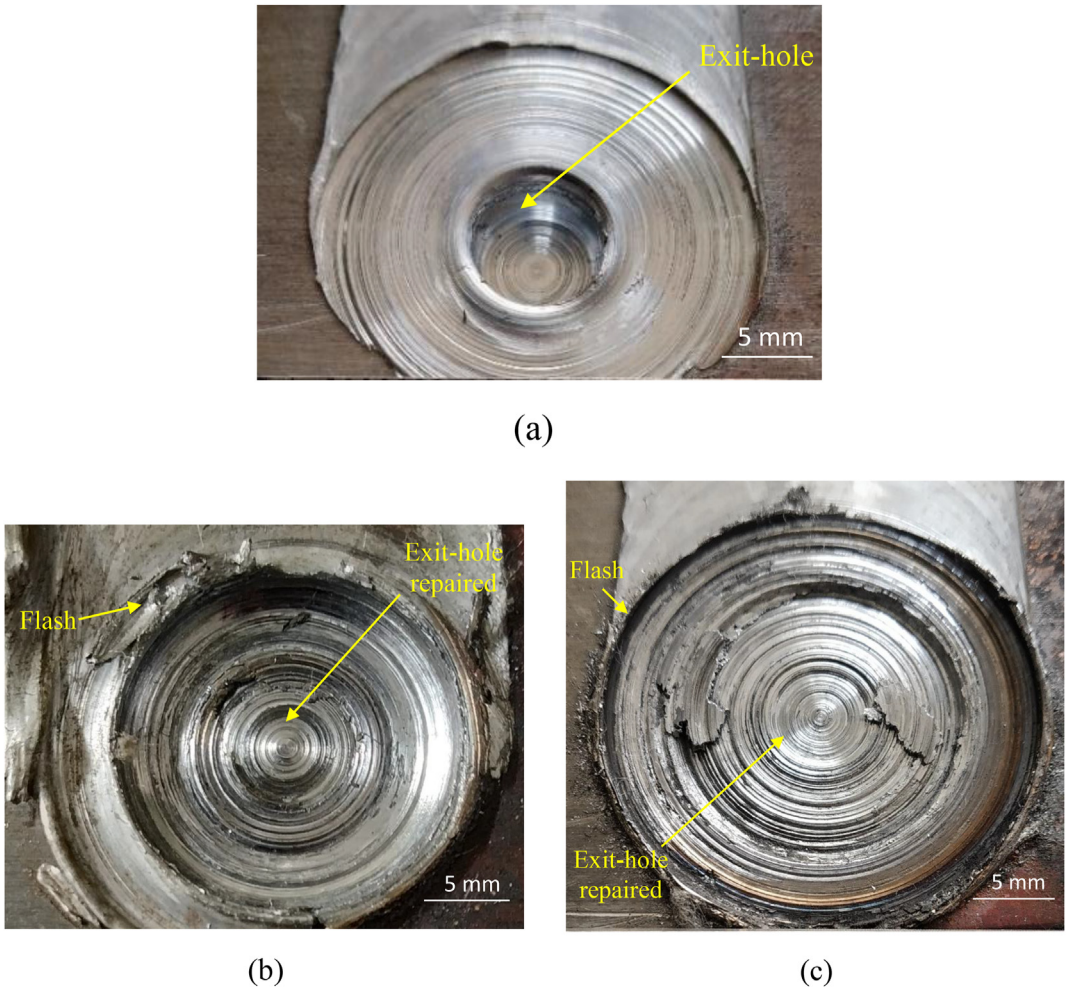

Fig. 3 – Surface crown appearance (a) exit-hole, (b) exit-hole repaired by shoulder diameters of 12 and 19 mm, and (c) exit-hole repaired by shoulder diameters of 12 and 27 mm.

second step by probeless tool of 27 mm shoulder diameter. Three samples are produced for each condition to observe the repeatability and consequent requirements for testing and characterization. From each condition, one sample is subjected to macrograph inspection, microstructure examination and hardness measurements, whereas other two samples are subjected to tensile testing.

After the welding and subsequent repairing, the samples are subjected to visual inspection, cross sectional macrographs, microstructure observations for the assessment of materials mixing, hardness measurements contours, and tensile testing. For the cross-sectional macrographs, the samples are sectioned from the center of the repaired zone as shown in Fig. 1 (Sez. A), whereas in case of welded zone's microstructure, the samples are sectioned from the transverse cross section of welded part as shown in Fig. 1 (Sez. B).

Specimens are extracted for microstructure, and microhardness characterization of the cross section orthogonal to the weld line of each joint. The specimens are mounted in a conductive thermoplastic resin and, subsequently, are lapped with grinding discs with final polishing using diamond paste of 1 μm particle size to achieve a mirror-like finishing. Samples are etched by using Keller etchant for 15 s to unveil the significant metallurgical features. An optical microscope, and a scanning electron microscope (SEM) equipped with an energy dispersive x-ray spectroscope (EDX) microprobe are used to observe the microstructure of the welding zones, and to detect presence of elements and subsequent formation of intermetallic compounds (IMCs). Vickers micro-hardness tests are carried out under an indentation load of 100 g for a dwell time of 15 s by using a Vickers Hardness Tester. The spacing between indentations is equal to 0.5 mm. The tensile testing specimens are extracted using wire cut electro discharge machining as per ASTM E8 mini tensile testing specimen standards, as shown in Fig. 2. The tensile testing is performed at 0.5 mm/min cross head speed, using universal tensile testing machine.

3. Results and discussion

3.1. *Visual inspection*

Figure 3 shows the surface crown appearance of exit-hole and repaired exit-hole, wherein three different images are shown such as: (a) exit-hole, (b) exit-hole repaired by shoulder

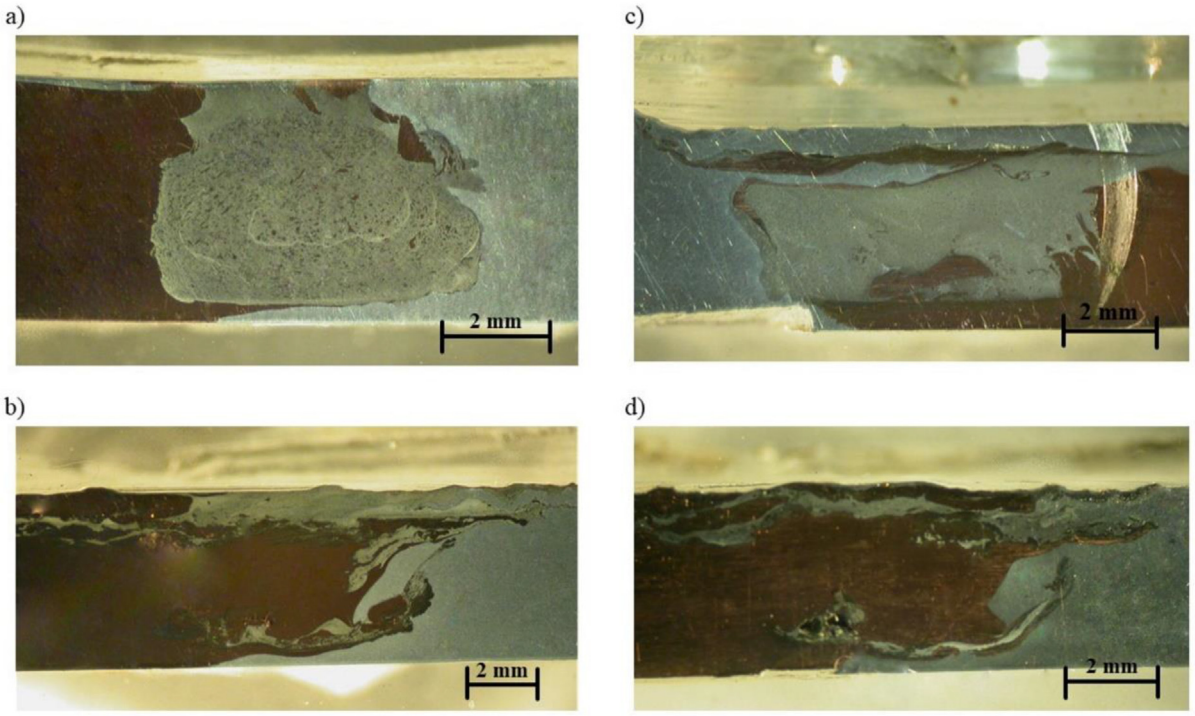

Fig. 4 – Cross sectional macrographs of (a) FS welded zone, (b) exit-hole repaired by shoulder diameters of 12 and 19 mm, and (c) and (d) exit-hole repaired by shoulder diameters of 12 and 27 mm.

diameters of 12 and 19 mm, and (c) exit-hole repaired by shoulder diameters of 12 and 27 mm. Fig. 3(b) and(c) show that the exit-hole is successfully repaired using non-consumable probeless tools, wherein the material adjacent to the exit-hole is plastically deformed and forged by probeless tools. In the case of exit-hole repaired by shoulder diameters of 12 and 19 mm as shown in Fig. 3(b), the flash is formed with the impression of the shoulder on the surface. The size of the impression is around 1 mm in depth. The shoulder impression and flash formation are less in case of exit-hole repaired by shoulder diameters of 12 and 27 mm as shown in Fig. 3(c) in comparison to Fig. 3(b). Increased shoulder size covers larger surface for materials participation in repairing that in turn resulted with better surface leveling with small shoulder impression and flash formation. In Fig. 3, no other surface discontinuities are observed on surface crown's based on visual inspection.

3.2. *Cross-sectional macrographs*

Figure 4 shows cross-sectional macrographs of FSW and repaired zone, wherein (a) FS welded zone, (b) exit-hole repaired by shoulder diameters of 12 and 19 mm, and (c) and (d) exit-hole repaired by shoulder diameters of 12 and 27 mm. Fig. 4(a) and (b) depict defect-free macrostructures, whereas voids are observed in Fig. 4(c) and (d) at the bottom side towards the Cu material. Additionally, Fig. 4(a) and (b) show three different macro zones, such as (i) processed zone, (ii) Cu base material and (iii) Al base material, whereas in case of Fig. 4(c) and (d), the processed zone is not distinctly observed. The voids in case of Fig. 4(c) and (d) are observed due to lack of materials consolidation and poor intermixing between Al and Cu materials. Another macroscopic difference between Fig. 4 (a–d) is the volume of materials participation during processing. Larger shoulder diameter of 27 mm in secondary repairing step leads to participation of Cu material in higher volume as compared to repairing step performed with shoulder diameter of 19 mm. Therefore, poor intermixing and lack of materials consolidation is strongly possible due to the participation of larger Cu and Al lumps in case of shoulder diameter of 27 mm. Besides, the processed regions in case of Fig. 4(a) and(b) are observed with small Cu fragments and better intermixing between Al and Cu materials. The materials mixing is furthermore discussed in subsequent section 3.3.

3.3. *Microstructure and materials mixing*

Figure 5 reports SEM images showing microstructures established within different regions of FS welded sample. The microstructures within weld region disclose two mix zones indicated as MIX 1 and MIX 2 in Fig. 5. In general, the microstructure of weld region consists of tiny Cu fragments that are dispersed from Cu base material and mixed in Al matrix material. However, the dispersion of tiny Cu fragments is heterogeneous throughout the thickness of workpieces and resulted with different MIX zones (such as MIX 1 and MIX 2) within weld zone region. In case of MIX 1 region, Cu fragments are evidenced as distinct in terms of size and shape, which are also distributed heterogeneously but with stirring features of onion ring type structure. On the other hand, for MIX 2 region, no such Cu fragments are evidenced. Also, this MIX 2 region is found above MIX 1 region (i.e. topmost region of weld zone). This region is more influenced by shoulder's stirring action

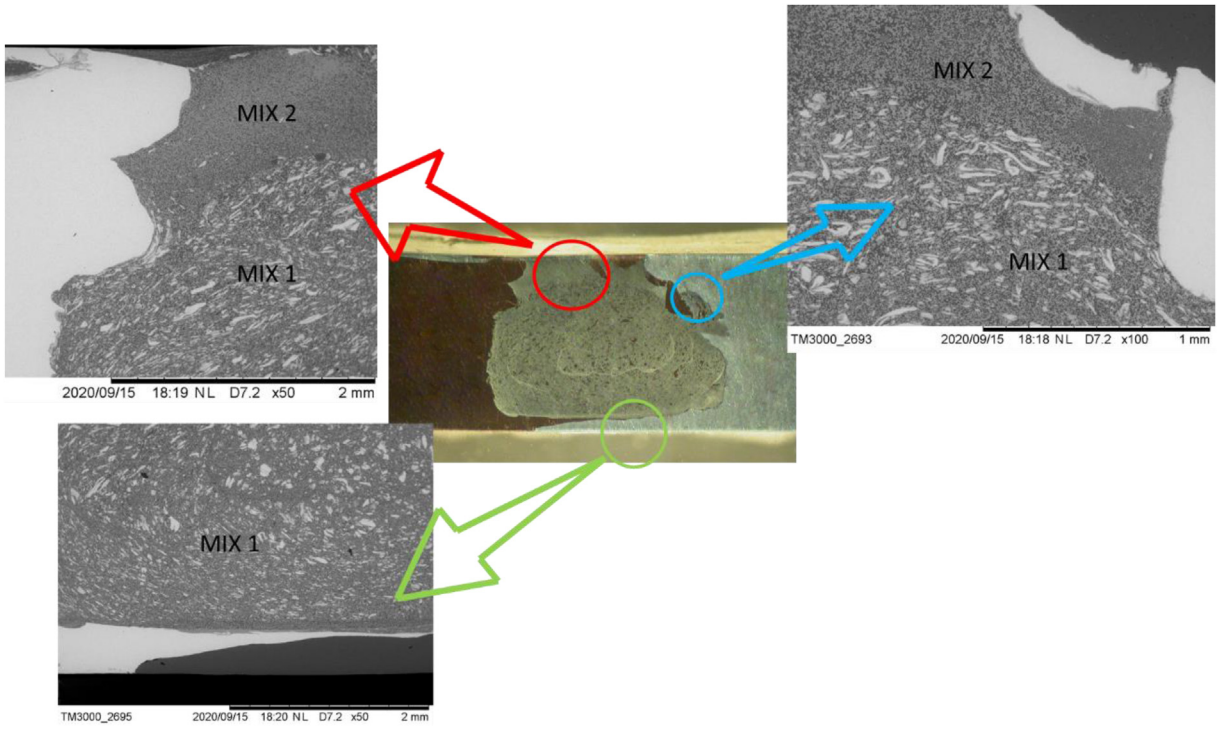

Fig. 5 – Microstructure images by SEM for different regions of FS welded sample.

and less by probe's stirring action. Therefore, the Cu fragments observed in case of MIX 1 are majorly dispersed from probe's stirring action. MIX 2 region is mainly consisting of Al matrix and few Cu fragments, whereas MIX 1 region consists of higher volume of Cu fragments mixed with Al matrix. The weld region is found defect free with appreciable materials mixing between Al and Cu. The similar type of materials mixing features are also found in previous literature of dissimilar FSW [1,4,19,20,22], which already resulted in substantially enhanced joint properties.

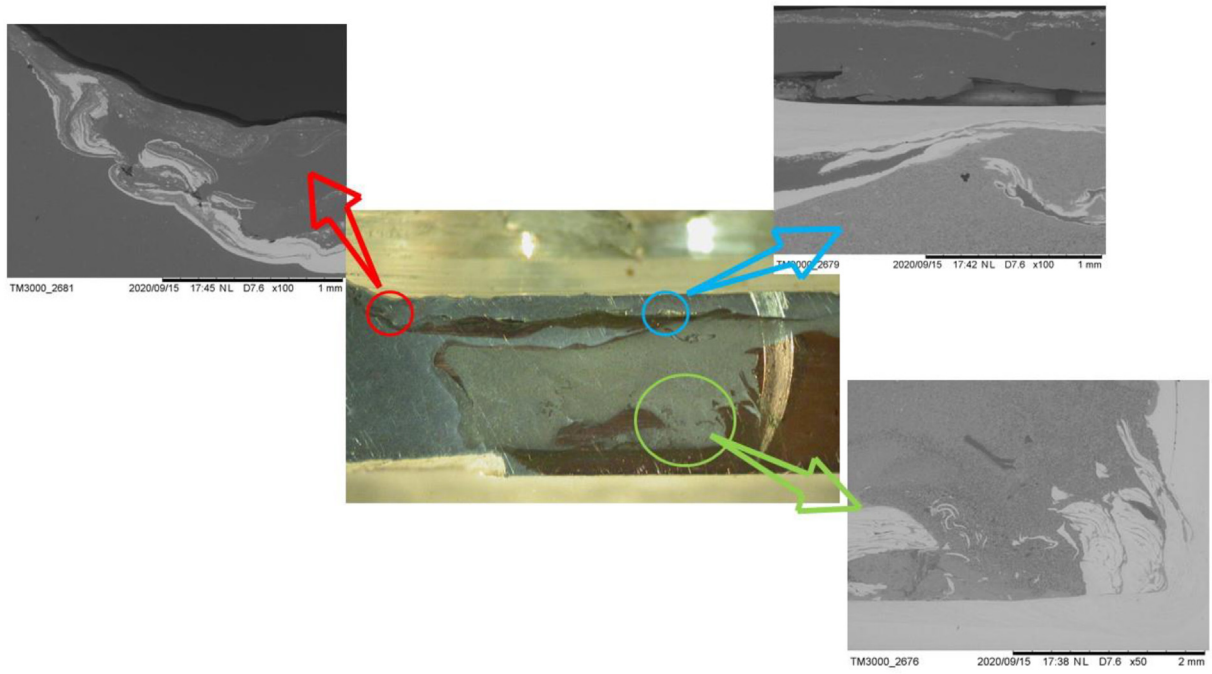

Fig. 6 – Microstructure images by SEM for different regions of exit-hole repaired by shoulder diameters of 12 and 19 mm.

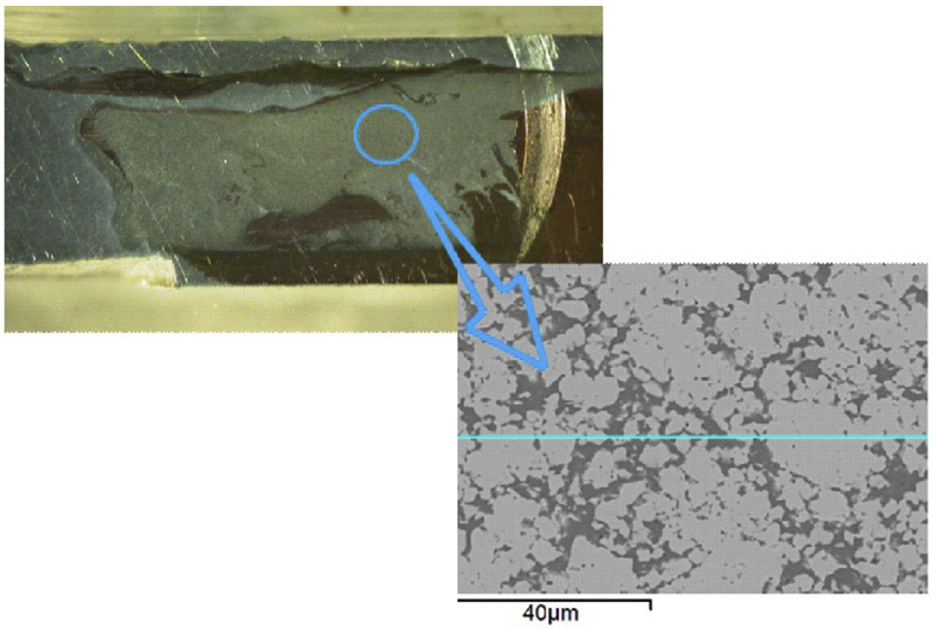

(a)

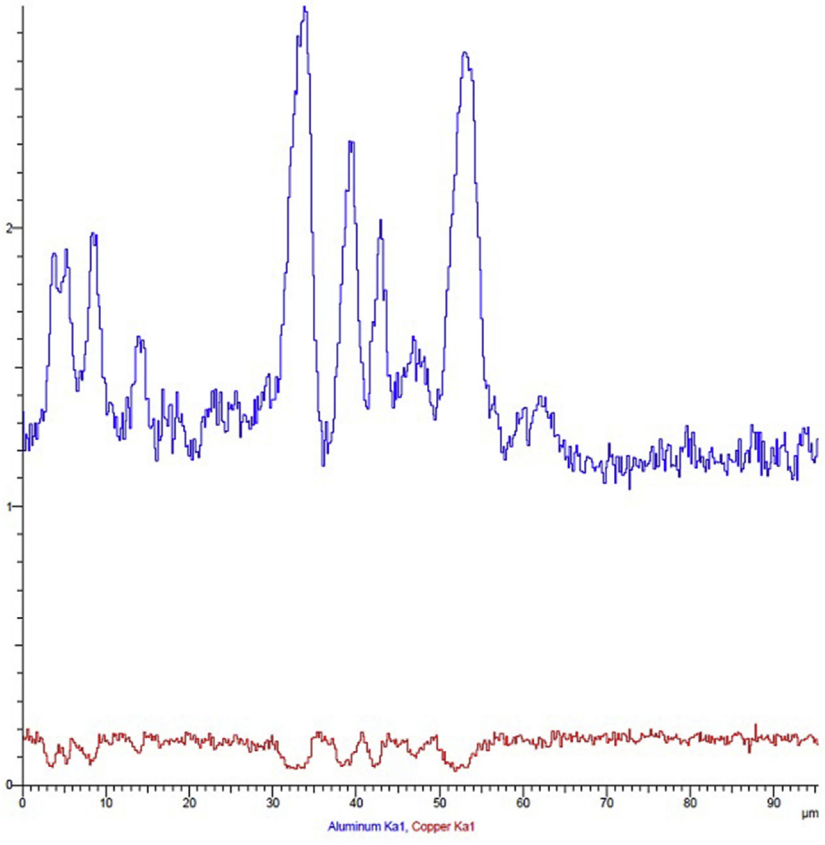

(b)

Fig. 7 – Materials mixing in exit-hole repaired zone processed by shoulder diameters of 12 and 19 mm: (a) macrograph and SEM image indicating scanning line for EDX, and (b) elemental mapping of Al and Cu for the line shown in (a).

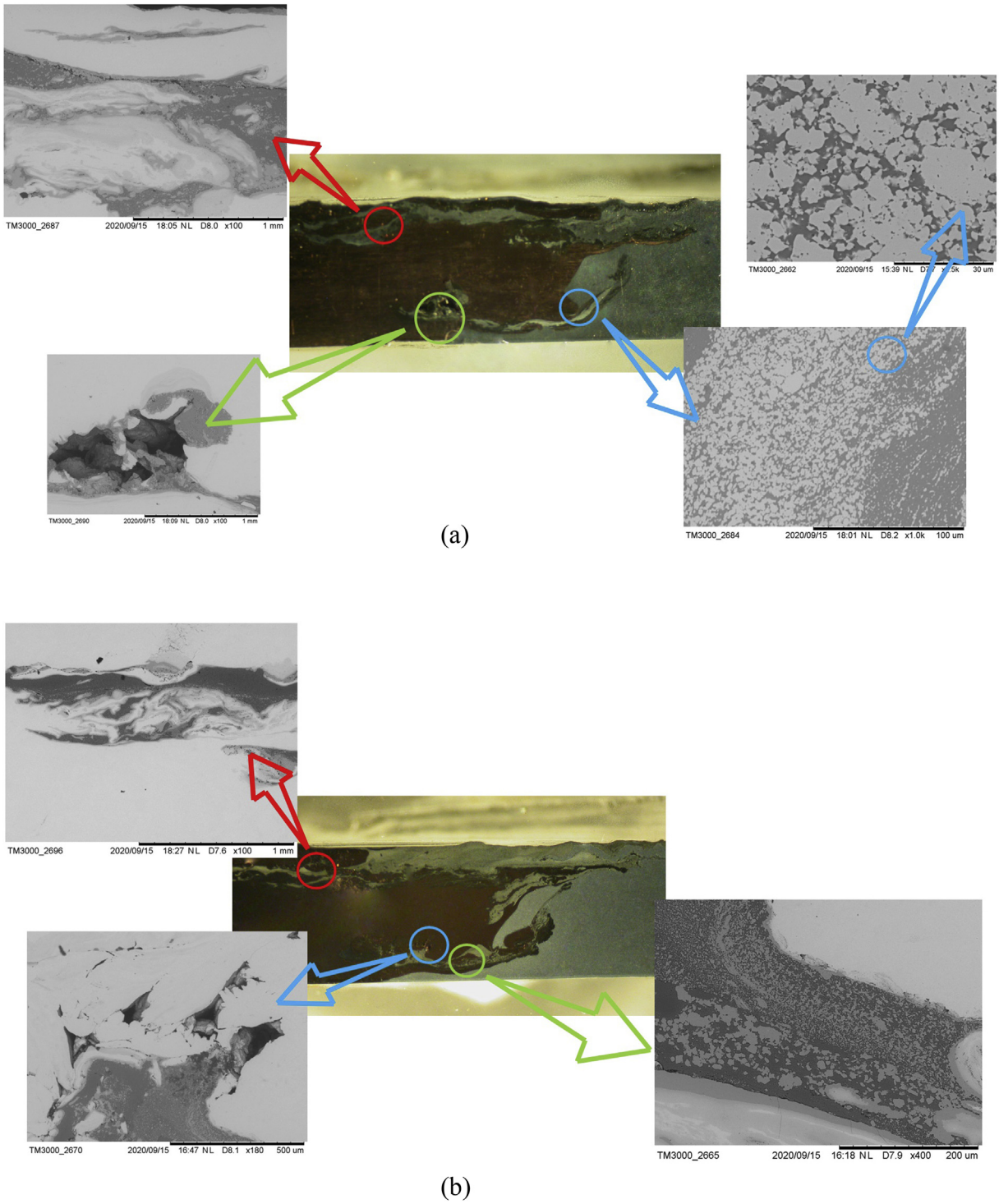

Fig. 8 – (a) and (b): Microstructure images by SEM for different regions of exit-hole repaired by shoulder diameters of 12 and 27 mm.

Fig. 6 shows SEM images to interpret microstructures for different exit-hole repaired regions in case of exit-hole repairing by shoulder diameters of 12 and 19 mm. The repaired zone is consisting of Cu fragments and Al matrix, but not similar to FS welded region. In this case of repairing, by probeless tools with 12 and19 mm shoulder diameters, the Cu fragments are larger as compared to the Cu fragments observed in FS welded region. This is due to bulk dispersion of Cu fragments induced by large shoulder surface contact of probeless tools on the peripheral material surrounded to the exit hole cavity. These Cu fragments and deformed Al materials are undergoing a softening followed by a plastic flow that are subjected to fill the exit-hole by actions of stirring (by shoulder's surface) and forging (with specified plunge rate)

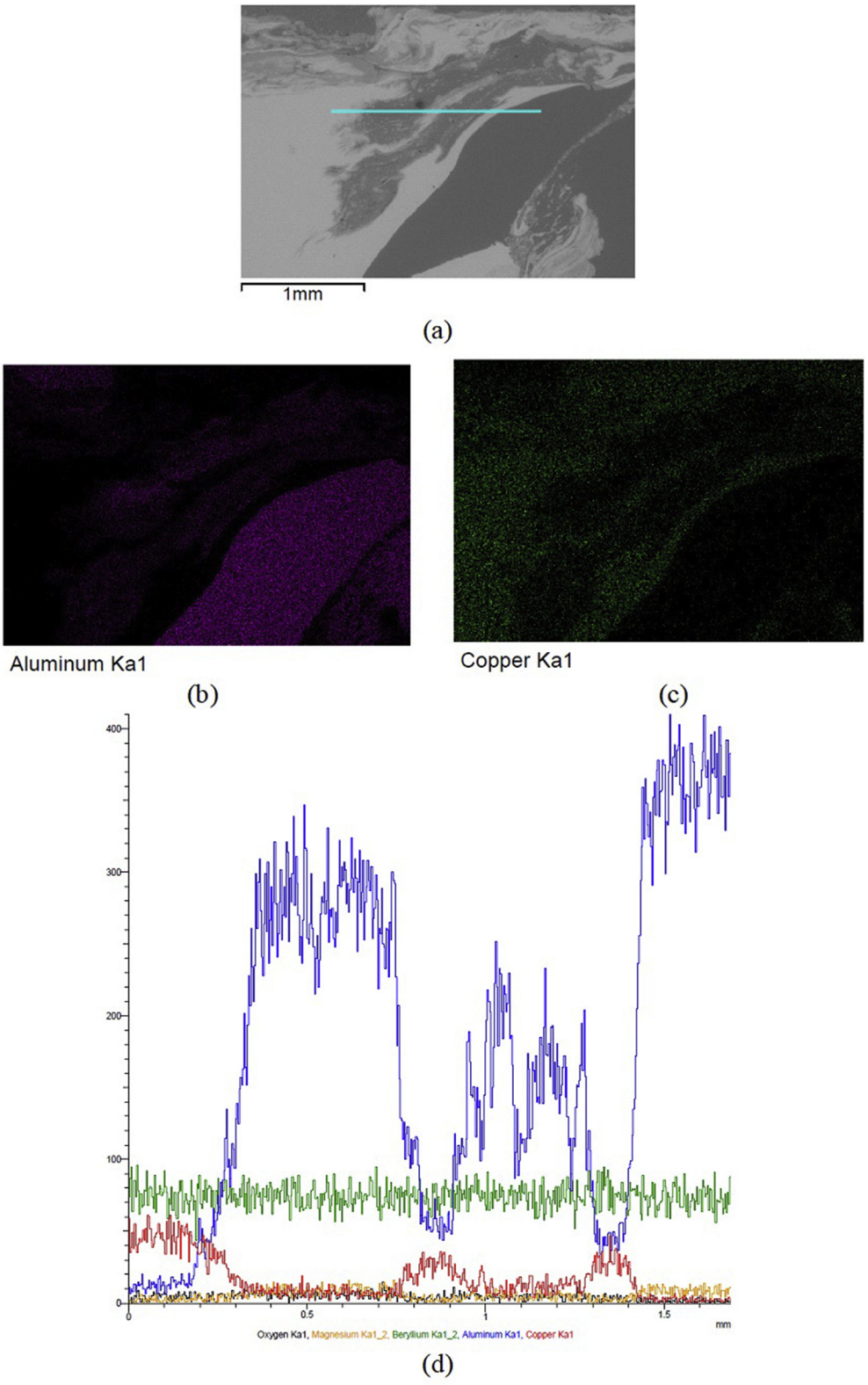

Fig. 9 – Materials mixing in exit-hole repaired zone processed by shoulder diameters of 12 and 27 mm corresponding to Fig. 8(a); (a) SEM image indicating scanning line for EDS, (b) and (c) area elemental mapping for image shown as (a), and elemental mapping of Al and Cu for the line shown in (a).

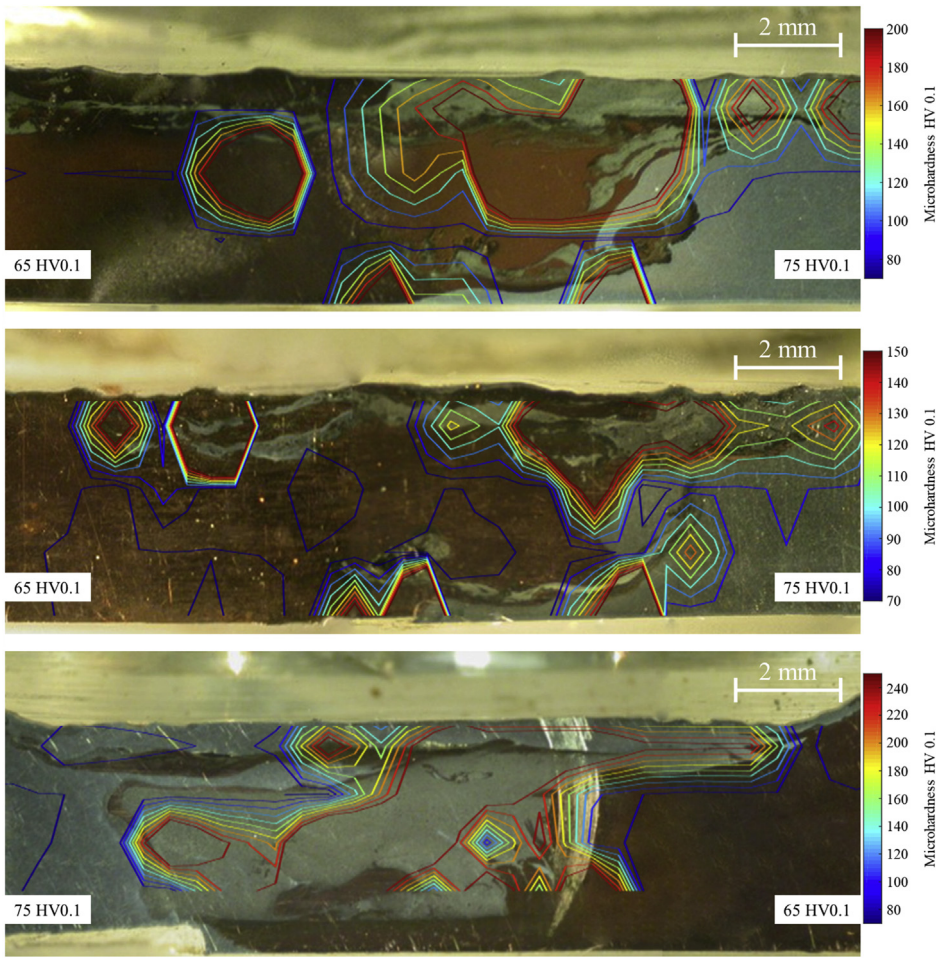

Fig. 10 – Hardness measurement contours for (a) exit-hole repaired zone processed by shoulder diameters of 12 and 19 mm, and (b) and (c) exit-hole repaired zone processed by shoulder diameters of 12 and 27 mm.

under the thermomechanical processing, wherein the Al and Cu materials are consolidated by solid state diffusion. Larger Cu fragments lead to poor materials mixing and consolidation, due to material flow restrictions caused by large Cu fragments in Al matrix although undergoing viscoplastic phase. Additionally, the metallurgical incompatibilities between Al and Cu mixing create defects in the processed region. Despite the involved issues and large fragments of Cu, appreciable materials mixing is obtained in the repaired zone having adequate materials participation from Al and Cu that are available surrounded the exit-hole and appropriate interfacial diffusion between them. Micro-voids are observed on top side of the repaired zone, whereas other regions within repaired zone are noticed as defect free. Appreciable materials mixing between Al and Cu is evidenced in Fig. 7, wherein the presence of Al and Cu elements can be observed in Fig. 7(b) for line shown in Fig. 7(a) with line mapping by EDX. The microstructure observed in Fig. 7(a) is majorly observed similarly in the middle of repaired zone, which is corresponding to the microstructure of MIX 2 observed in Fig. 5, whereas bulk Cu fragments mixed with Al matrix are observed at top and bottom of repaired zone. The presence of Al and Cu elements observed in Fig. 7(a) indicates the mixing between Al and Cu elements with formation of intermetallic compounds (IMCs) in the repaired zone [46,47].

Fig. 8 shows SEM images to interpret microstructures for different exit-hole repaired regions in case of exit-hole repairing by shoulder diameters of 12 and 27 mm, wherein (a) and (b) are processed with same processing parameters. The repaired zone is majorly covered by bulk Cu, which is transported by the large contact surface of shoulder diameter 27 mm. Defects such as voids and cracks are also observed at the bottom of repaired zone. This is believed to be due the larger shoulder diameter causing increased dispersion of Cu bulk fragments through larger contact surface, that in turn leads to material flow restrictions in the Al matrix. Inadequate materials mixing consisting of metallurgical incompatibilities between bulky Cu fragments and Al material have caused defects such as voids and cracks in the processed region, wherein lack of material consolidation can be observed from Fig. 8. Some material mixing between Al and Cu is observed in small regions within processed zone (mostly towards bottom

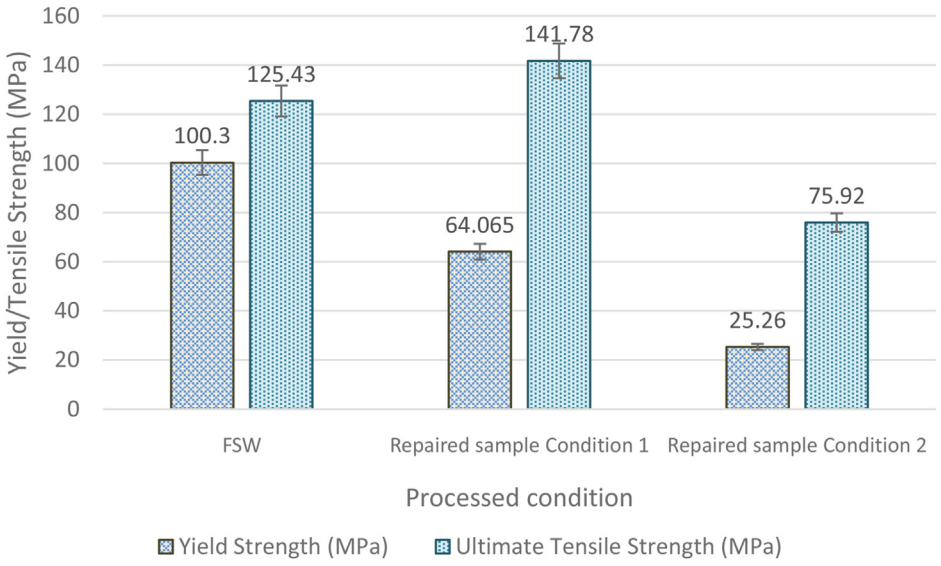

Fig. 11 – Tensile testing results of processed samples, FSW, exit-hole repaired by shoulder diameters of 12 and 19 mm (repaired sample condition 1), and exit-hole repaired by shoulder diameters of 12 and 27 mm (repaired sample condition 2).

region of repaired zone), which are microstructures corresponding to MIX 2 in Fig. 5. At the bottom side interface between Al–Cu materials within repaired zone, the IMCs layer can be seen from Fig. 8(a) and (b), which is formed probably due to solid state diffusion. The material mixing between Al and Cu within processed regions is also observed at top region with interpenetrated features of Al and Cu fragments as can be seen from Fig. 9. The presence of Al and Cu elements in Fig. 9(b) and (c) is observed as bulk fragments of both the materials, wherein the interface between these fragments may be consisting of IMCs of Al–Cu binary phase as can be seen from Fig. 9(d). It can also be seen from Fig. 9(d) that, the Al and Cu elements are intermixed with each other at the top region of repaired zones. Overall, limited material mixing between Al and Cu is observed in case of exit-hole repairing by shoulder diameters of 12 and 27 mm, whereas bulk fragments of Cu and Al are observed in the repaired zone with defects such as voids and cracks. Therefore, larger shoulder diameter such as 27 mm as compared to another shoulder diameter of 19 mm (however, equal to FSW's tool shoulder diameter) is not recommended for repairing of exit-hole (around 8 mm diameter) due to dispersion of large bulky Cu fragments and poor consolidation from the stirring action.

3.4. *Hardness measurements and contour plots*

Figure 10 shows hardness measurements and contour plots for exit-hole repaired samples. The hardness contours confirm heterogeneity within repaired zone that is also observed in microstructure features shown in previous section. The sample of exit-hole repaired by shoulder diameters of 12 and 19 mm is observed in Fig. 10(a), with maximum hardness of 240 HV0.1 at the interface between Cu base material and processed region, which can be caused by the formation of hard and brittle IMCs at that zone. In previous literature of Al–Cu FSW [46,47], the IMCs are observed at the interface between weld zone and Cu base material due to its inherent nature of brittle behavior and generally have high hardness typically from complex crystal microstructures. The central region of processed zone is also noticeable with high hardness contour, which is also possibly due to the formation of IMCs. In this sample of exit-hole repaired by shoulder diameters of 12 and 19 mm, the intermixing between Al and Cu is evidenced at the processed region with maximum hardness. There are some regions noticed with hardness contours in between 140 and 100 HV0.1, wherein the fragments from

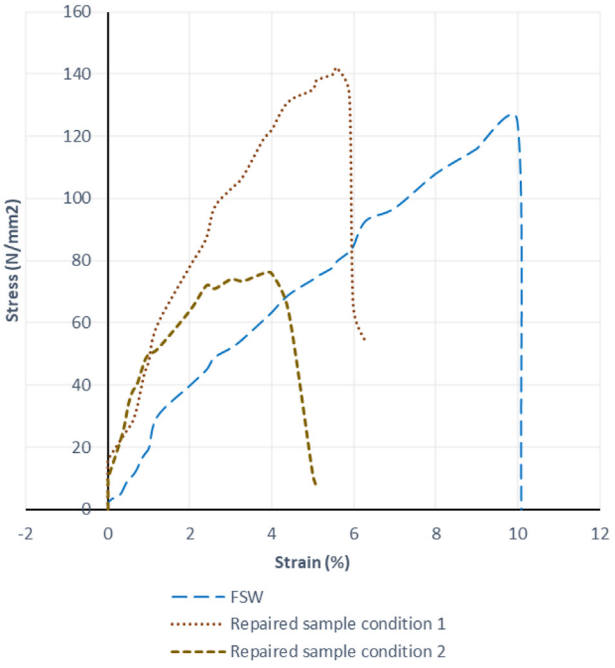

Fig. 12 – The stress–strain curves for tensile testing of FSW and exit-hole repaired samples.

base materials are plastically deformed and experienced the strain hardening under the effect of thermomechanical processing.

Fig. 10(b) and (c) show hardness measurements and contour plots for samples of exit-hole repaired by shoulder diameters of 12 and 27 mm. As the repaired zone is covered by large bulky Cu fragments, the hardness contours at the center of the repaired zone are different and consist of lower hardness as compared to the ones that are observed for the sample of exit-hole repaired by shoulder diameters of 12 and 19 mm. Maximum hardness is noticed at the interface between Cu–Al within repaired zone, mostly towards the top of repaired zone, in both two samples of exit-hole repaired by shoulder diameters of 12 and 27 mm. The materials mixing between Al–Cu elements are observed at these regions, wherein hardness is reasonably higher due to formation of IMCs. Large bulky Cu fragments in the center region of repaired zone is observed with hardness contours in between 140 and 80 HV0.1, wherein the material has experienced plastic deformation and strain hardening under thermo mechanical processing. Inadequate materials mixing and presence of large bulky Cu fragments lead to more heterogeneous hardness contour plots as can be observed from Fig. 10(b) and (c) in case of exit-hole repaired by shoulder diameters of 12 and 27 mm.

The hardness counters of repaired zone are observed within the similar range of hardness reported for friction stir welded zone in [8–10]. This shows the materials mixing phenomenon is like the processed zones observed in case of FSW, with similar possible formation of IMCs. This may be caused by the similar temperature range that the processing region is experiencing during repairing as compared to the materials of processing zone for FSW process, wherein both the processes are solid state processing that operates under the effect of plastic deformation and subsequent viscoplastic material flow.

3.5. *Tensile testing*

Figure 11 shows tensile testing results of processed samples such as FS welded sample, exit-hole repaired sample processed by shoulder diameters of 12 and 19 mm, and 12 and 27 mm. Maximum ultimate tensile strength of 141.8 MPa is obtained for exit-hole repaired sample processed by shoulder diameters of 12 and 19 mm, which is 13% higher as compared to FS welded region (125.4 MPa). Minor difference in ultimate tensile strength between FS welded and exit-hole repaired regions can be attributed to differences in materials mixing caused by two different processing ways. In the exit-hole repairing by shoulder diameters of 12 and 19 mm, the multiaxial forging in the cavity of exit-hole, with enhanced bonding inside the repaired zone, is more pronounced as compared to FS welded region. This may be the origin of the 13% increase in ultimate tensile strength. At least for this specific 8 mm exit-hole diameter, the exit-hole repairing by shoulder diameters of 12 and 19 mm is therefore recommended. The yield strength of 64.1 MPa is observed for exit-hole repaired by shoulder diameters of 12 and 19 mm, which is lower as compared to FS welded sample (100.3 MPa). This may be due to localized harder zones, within the repaired region, that trigger early localized strain mechanisms starting the plastic deformation. Besides, ultimate tensile strength of 75.9 MPa and yield strength of 25.3 MPa are received for exit-hole repaired zone by shoulder diameters of 12 and 27 mm. Inadequate materials mixing between Al and Cu in addition to the presence of defects such as voids and cracks in the repaired region also lead to low tensile strength.

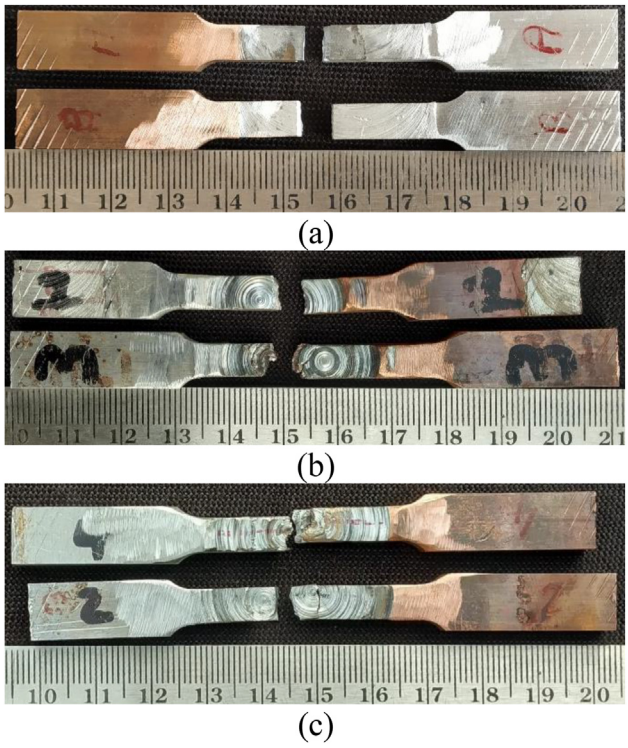

Fig. 13 – The fractured tensile specimens: (a) FSW, (b) exit-hole repaired by shoulder diameters of 12 and 19 mm (repaired sample condition 1), and exit-hole repaired by shoulder diameters of 12 and 27 mm (repaired sample condition 2).

Fig. 12 shows the stress–strain curves for tensile testing of FSW and exit-hole repaired samples. Although the exit-hole repaired sample processed by shoulder diameters of 12 and 19 mm presents higher tensile strength, the elongation at fracture is reduced to 5.6%, from the 10% maximum elongation observed in case of FSW tensile testing. This may be due to the increased IMCs in the case of exit-hole repaired sample processed by shoulder diameters of 12 and 19 mm as compared to FSW sample. The lowest elongation among the three investigated conditions, with 4.75%, is observed for the exit-hole repaired sample processed by shoulder diameters of 12 and 27 mm. This can be attributed to the presence of defects, such as voids and cracks, observed in the processed region. The fracture location of tensile specimens can be seen

from Fig. 13. The FSW samples are fractured from the interface between Cu and weld zone, whereas the repaired samples are fractured from the center of the processed zone, as it would be expectable from an axisymmetric processing without the travel speed component. In case of exit-hole repaired sample processed by shoulder diameters of 12 and 19 mm, the fracture location is in the processed zone but initiated from the surrounding of large Cu fragments within repaired zone, as depicted from Fig. 13(b). In a different way, in case of exit-hole repaired sample processed by shoulder diameters of 12 and 27 mm, the fracture location is from the defects, as evidenced by Fig. 13 (c).

4. Conclusions

The exit-hole in dissimilar Al–Cu FSW is successfully repaired in two processing steps by probeless non-consumable tools without addition of consumable materials or any edge preparation. The repairing of the dissimilar Al–Cu FSW's exit-hole is performed by plunging probeless tools in the exit-hole and its surrounding zone to obtain participation of the same Al and Cu base materials in the cavity of exit-hole, wherein thermomechanical processing is responsible for materials mixing and joint consolidation. The results obtained from the repaired samples, in terms of materials mixing and properties, are compared with the properties of the joints from FSW. Following conclusions are drawn from this investigation:

1) The materials mixing between Al and Cu in the repairing zone of exit-hole is affected by the shoulder diameter. Higher volume of Al is involved in the repairing zone in case of repairing by shoulder diameters of 12 and 19 mm, while higher volume of Cu is involved in the repairing zone in case of shoulder diameters of 12 and 27 mm.
2) Increased participation of Cu in exit-hole repairing leads to the presence of large bulky fragments in the repaired zone impairing a sound material flow leading to formation of defects such as micro-voids and cracks are observed in case of repairing with shoulder diameters of 12 and 27 mm.
3) Appreciable intermixing between Al and Cu is observed in case of repairing zone when applying the shoulder diameters of 12 and 19 mm. The weld zone of the friction stir welded region consists of tiny Cu fragments stirred by the probe of the tool and mixed with Al matrix.
4) The exit-hole repaired with shoulder diameters of 12 and 19 mm obtained an ultimate tensile strength 13% higher than the FS welded region.
5) The maximum and minimum hardness of the repair zone made with shoulder diameters of 12 and 19 mm are 240 and 80 HV0.1, respectively, which are within the same range of FSW region of previously published investigations.

Declaration of Competing Interest

The authors declare that they have no known competing financial interests or personal relationships that could have appeared to influence the work reported in this paper.

Acknowledgements

Authors gratefully acknowledge Eng. Hetal Parmar for her support and dedication shown during the experimental activities. Kush Mehta is thankful to School of Engineering, Aalto University, Finland for postdoctoral researcher's scholarship.

REFERENCES

[1] Mehta KP. A review on friction-based joining of dissimilar aluminum – steel joints. J Mater Res 2019;34:78–96. https://doi.org/10.1557/jmr.2018.332.

[2] Mehta KP, Badheka VJ. A review on dissimilar friction stir welding of copper to aluminum: process, properties, and variants. Mater Manuf Process 2016;31:233–54. https://doi.org/10.1080/10426914.2015.1025971.

[3] Mehta KP, Carlone P, Astarita A, Scherillo F, Rubino F. Conventional and cooling assisted friction stir welding of AA6061 and AZ31B alloys. Mater Sci Eng, A 2019;759:252–61. https://doi.org/10.1016/j.msea.2019.04.120.

[4] Carlone P, Astarita A, Palazzo GS, Paradiso V, Squillace A. Microstructural aspects in Al–Cu dissimilar joining by FSW. Int J Adv Manuf Technol 2015;79:1109–16. https://doi.org/10.1007/s00170-015-6874-z.

[5] Ólafsson D, Vilaça P, Vesanko J. Multiphysical characterization of FSW of aluminum electrical busbars with copper ends. Weld World 2020;64:59–71. https://doi.org/10.1007/s40194-019-00814-0.

[6] Shankar S, Vilaça P, Dash P, Chattopadhyaya S, Hloch S. Joint strength evaluation of friction stir welded Al-Cu dissimilar alloys. Measurement 2019;146:892–902. https://doi.org/10.1016/j.measurement.2019.07.019.

[7] Mehta KP, Vilaça P. A review on friction stir-based channeling. 0 Crit Rev Solid State Mater Sci 2021:1–45. https://doi.org/10.1080/10408436.2021.1886042.

[8] Ipekoğlu G, Erim S, Gören Kiral B, Çam G. Investigation into the effect of temper condition on friction stir weldability of AA6061 Al-alloy plates. Kov Mater 2013;51:155–63. https://doi.org/10.4149/km.2013.3.155.

[9] Heidarzadeh A, Mironov S, Kaibyshev R, Çam G, Simar A, Gerlich A, et al. Friction stir welding/processing of metals and alloys: a comprehensive review on microstructural evolution. Prog Mater Sci 2020;117:100752. https://doi.org/10.1016/j.pmatsci.2020.100752.

[10] Çam G. Friction stir welded structural materials: beyond Al-alloys. Int Mater Rev 2011;56:1–48. https://doi.org/10.1179/095066010X12777205875750.

[11] Kashaev N, Ventzke V, Çam G. Prospects of laser beam welding and friction stir welding processes for aluminum airframe structural applications. J Manuf Process 2018;36:571–600. https://doi.org/10.1016/j.jmapro.2018.10.005.

[12] Ipekoğlu G, Kiral BG, Erim S, Çam G. Investigation of the effect of temper condition on the friction-stir weldability of AA7075 Al-alloy plates. Mater Tehnol 2012;46:627–32.

[13] Çam G, Mistikoglu S, Pakdil M. Microstructural and mechanical characterization of friction stir butt joint welded 63% Cu-37% Zn brass plate. Weld J (Miami, Fla) 2009;88.

[14] Ipekoglu G, Erim S, Cam G. Investigation into the influence of post-weld heat treatment on the friction stir welded AA6061 Al-Alloy plates with different temper conditions. Metall Mater Trans A Phys Metall Mater Sci 2014;45:864–77. https://doi.org/10.1007/s11661-013-2026-y.

[15] Çam G, Serindağ HT, Çakan A, Mistikoglu S, Yavuz H. The effect of weld parameters on friction stir welding of brass plates. Mater Werkst 2008;39:394–9. https://doi.org/10.1002/mawe.200800314.
[16] Çam G, İpekoğlu G. Recent developments in joining of aluminum alloys. Int J Adv Manuf Technol 2017;91:1851–66. https://doi.org/10.1007/s00170-016-9861-0.
[17] Cam G, Ipekoglu G, Tarik Serindag H. Effects of use of higher strength interlayer and external cooling on properties of friction stir welded AA6061-T6 joints. Sci Technol Weld Join 2014;19:715–20. https://doi.org/10.1179/1362171814Y.0000000247.
[18] Patel NP, Parlikar P, Dhari RS, Mehta K, Pandya M. Numerical modelling on cooling assisted friction stir welding of dissimilar Al-Cu joint. J Manuf Process 2019;47:98–109. https://doi.org/10.1016/j.jmapro.2019.09.020.
[19] Mehta KP, Badheka VJ. Effects of tilt angle on the properties of dissimilar friction stir welding copper to aluminum. Mater Manuf Process 2016;31:255–63. https://doi.org/10.1080/10426914.2014.994754.
[20] Mehta KP, Badheka VJ. Hybrid approaches of assisted heating and cooling for friction stir welding of copper to aluminum joints. J Mater Process Technol 2017;239:336–45. https://doi.org/10.1016/j.jmatprotec.2016.08.037.
[21] Mehta KP, Badheka VJ. Influence of tool design and process parameters on dissimilar friction stir welding of copper to AA6061-T651 joints. Int J Adv Manuf Technol 2015;80:2073–82. https://doi.org/10.1007/s00170-015-7176-1.
[22] Mehta KP, Badheka VJ. Influence of tool pin design on properties of dissimilar copper to aluminum friction stir welding. Trans Nonferrous Met Soc China 2017;27:36–54. https://doi.org/10.1016/S1003-6326(17)60005-0.
[23] Huang Y, Xie Y, Meng X, Li J, Zhou L. Joint formation mechanism of high depth-to-width ratio friction stir welding. J Mater Sci Technol 2019;35:1261–9. https://doi.org/10.1016/j.jmst.2019.01.016.
[24] Huang Y, Xie Y, Meng X, Lv Z, Cao J. Numerical design of high depth-to-width ratio friction stir welding. J Mater Process Technol 2018;252:233–41. https://doi.org/10.1016/j.jmatprotec.2017.09.029.
[25] Zettler R, Vugrin T. Effects and defects of friction stir welds. In: Lohwasser D, Chen Z, editors. Frict. Stir weld. From basics to appl.; 2003. p. 245–76.
[26] Mehta K. Advanced joining and welding techniques: an overview. In: Gupta K, editor. Adv. Manuf. Technol. Mater. Forming. Mach. Tribol.; 2017. p. 101–36. https://doi.org/10.1007/978-3-319-56099-1.
[27] Mishra RS, De PS, Kumar N. Friction stir processing: science and engineering. 2014. https://doi.org/10.1007/978-3-319-07043-8.
[28] Vilaça P, Thomas W. Friction stir welding technology. In: Moreira PMGP, Da Silva LFM, Paulo de CMST, editors. Struct. Connect. Light. Met. Struct. Adv. Struct. Mater.; 2011. p. 85–124. https://doi.org/10.1007/8611.
[29] ISO 25239-1:2020 International organization for standardization. 2020.
[30] Meng X, Huang Y, Cao J, Shen J, dos Santos JF. Recent progress on control strategies for inherent issues in friction stir welding. Prog Mater Sci 2021;115:100706. https://doi.org/10.1016/j.pmatsci.2020.100706.
[31] Vilaça P, Mendes J, Nascimento F, Quintino L. Application of FSW to join aluminium foil winding coils for electrical transformers. Int J Mech Syst Eng 2016;2. https://doi.org/10.15344/2455-7412/2016/115.
[32] Behmand SA, Mirsalehi SE, Omidvar H, Safarkhanian MA. Filling exit holes of friction stir welding lap joints using consumable pin tools. Sci Technol Weld Join 2015;20:330–6. https://doi.org/10.1179/1362171815Y.0000000018.
[33] Huang YX, Han B, Tian Y, Liu HJ, Lv SX, Feng JC, et al. New technique of filling friction stir welding. Sci Technol Weld Join 2011;16:497–501. https://doi.org/10.1179/1362171811Y.0000000032.
[34] Xu Z, Li Z, Ji S, Zhang L. Refill friction stir spot welding of 5083-O aluminum alloy. J Mater Sci Technol 2018;34:878–85. https://doi.org/10.1016/j.jmst.2017.02.011.
[35] Ji S, Meng X, Zeng Y, Ma L, Gao S. New technique for eliminating keyhole by active-passive filling friction stir repairing. Mater Des 2016;97:175–82. https://doi.org/10.1016/j.matdes.2016.02.088.
[36] Ji SD, Meng XC, Huang RF, Ma L, Gao SS. Microstructures and mechanical properties of 7N01-T4 aluminum alloy joints by active-passive filling friction stir repairing. Mater Sci Eng, A 2016;664:94–102. https://doi.org/10.1016/j.msea.2016.03.131.
[37] Wen Q, Guo R, Song Q, Dong Z, Liu G, Huang R, et al. Active-passive filling friction stir repairing of casting defects in ZL210 aluminum alloys. Int J Adv Manuf Technol 2020;106:5307–15. https://doi.org/10.1007/s00170-020-05026-1.
[38] Zhou L, Liu D, Nakata K, Tsumura T, Fujii H, Ikeuchi K, et al. New technique of self-refilling friction stir welding to repair keyhole. Sci Technol Weld Join 2012;17:649–55. https://doi.org/10.1179/1362171812Y.0000000058.
[39] Han B, Huang Y, Lv S, Wan L, Feng J, Fu G. AA7075 bit for repairing AA2219 keyhole by filling friction stir welding. Mater Des 2013;51:25–33. https://doi.org/10.1016/j.matdes.2013.03.089.
[40] Mehta KP, Patel R. On fsw keyhole removal to improve volume defect using pin less tool. Key Eng Mater 2019;821:KEM:215. https://doi.org/10.4028/www.scientific.net/KEM.821.215. 21.
[41] Mehta KP, Patel R, Vyas H, Memon S, Vilaça P. Repairing of exit-hole in dissimilar Al-Mg friction stir welding: process and microstructural pattern. Manuf Lett 2020;23:67–70. https://doi.org/10.1016/j.mfglet.2020.01.002.
[42] Memon S, Paidar M, Mehta KP, Babaei B, Lankarani HM. Friction spot extrusion welding on dissimilar materials AA2024-T3 to AA5754-O: effect of shoulder plunge depth. J Mater Eng Perform 2021;30:334–45. https://doi.org/10.1007/s11665-020-05387-4.
[43] Han J, Paidar M, Vignesh RV, Mehta KP, Heidarzadeh A, Ojo OO. Effect of shoulder features during friction spot extrusion welding of 2024-T3 to 6061-T6 aluminium alloys. Arch Civ Mech Eng 2020;20:1–17. https://doi.org/10.1007/s43452-020-00086-2.
[44] Haiyan Z, Mehta KP. Effect of materials positioning on dissimilar modified friction stir clinching between aluminum 5754-O and 2024-T3 sheets. Vacuum 2020;178:109445. https://doi.org/10.1016/j.vacuum.2020.109445.
[45] Gao P, Zhang Y, Mehta KP. Metallurgical and mechanical properties of Al–Cu joint by friction stir spot welding and modified friction stir clinching. Met Mater Int 2020. https://doi.org/10.1007/s12540-020-00759-w.
[46] Heideman R, Johnson C, Kou S. Metallurgical analysis of Al/Cu friction stir spot welding. Sci Technol Weld Join 2010;15:597–604. https://doi.org/10.1179/136217110X12785889549985.
[47] Kah P, Vimalraj C, Martikainen J, Suoranta R. Factors influencing Al-Cu weld properties by intermetallic compound formation. Int J Mech Mater Eng 2015;10. https://doi.org/10.1186/s40712-015-0037-8.